Materials Research Express

PAPER

Thermally stimulated relaxation and behaviors of oxygen vacancies in $SrTiO_3$ single crystals with (100), (110) and (111) orientations

Haimo Qu[1], **Bingcheng Luo**[2], **Shuaishuai Bian**[1] **and Zhenxing Yue**[1]

[1] State Key Laboratory of New Ceramics and Fine Processing, School of Materials Science and Engineering, Tsinghua University, Beijing, 100084, People's Republic of China
[2] Department of Engineering, University of Cambridge, CB3 0FA Cambridge, United Kingdom

E-mail: yuezhx@mail.tsinghua.edu.cn

Keywords: $SrTiO_3$, TSDC, first-principles, oxygen vacancy, defect relaxation

OPEN ACCESS

RECEIVED
26 February 2020

REVISED
24 March 2020

ACCEPTED FOR PUBLICATION
3 April 2020

PUBLISHED
14 April 2020

Abstract

The strontium titanate ($SrTiO_3$) single crystals with different orientations of (100), (110) and (111) were investigated using thermally stimulated depolarization current (TSDC) measurements, which has been proved to be an effective strategy to fundamentally study the relationship between relaxation phenomena and defect chemistry in dielectrics. The origins of different relaxations in $SrTiO_3$ crystals were identified and the activation energy of oxygen vacancies was estimated from TSDC measurements. It was further found that oxygen-treated $SrTiO_3$ crystals exhibit different relaxation behaviors. Noticeable changes of thermal relaxation associated with oxygen vacancies have taken place in relation to the crystalline anisotropy. The $SrTiO_3$ (110) samples display higher concentration and activation energy of oxygen vacancies. First-principles calculations were carried out on $SrTiO_3$ (110) crystals to study the effect of oxygen vacancy on different surface microstructure. From the resulting minimum formation energy of 0.63 eV, it demonstrates that the oxygen vacancies tend to form on the TiO-terminated surfaces. Considering the band structure, oxygen vacancies near the surface contribute to the transition of crystal from insulator to metallic characteristic.

1. Introduction

The breathtaking progress in communication and new energy technology has led an ever higher growth of demand for perovskite oxides used as dynamics random access memories, multilayer ceramic capacitors (MLCCs), multilayer actuators, and other electroceramic components with a wide range of applications [1, 2]. Strontium titanate ($SrTiO_3$) is a well-known versatile, low-cost perovskite oxide. It has been widely applied into capacitors, varistors, thermistors and semiconductor photocatalyst owing to its high dielectric and incipient ferroelectric response, good thermal and chemical stability, and photocorrosion resistibility [3–6]. The primary defects considered in ABO_3 perovskite are singly and doubly ionized acceptor dopants A′, A″ and shallow donors oxygen vacancies $V_O^{\cdot\cdot}$, rather than electronic carriers [7]. Additionally, the transformation of Ti^{4+} to Ti^{3+} in Ti-containing dielectrics, which is known as the coring effect, seems to be unavoidable during high-temperature sintering [8, 9]. It was generally confirmed that the defect chemistry [10] including the formation and motion of oxygen vacancies determines various dielectric effects such as conductivity, activation energy, second harmonic generation efficiency [11], loss and failure mechanisms [2] of perovskite oxides or other types of crystals. Hou *et al* made full use of the ion interdiffusion and redistribution of oxygen vacancies at STO/LSMO interface, thus significantly enhancing the E_b of Au/STO/LSMO capacitors under positive electric field and leading to an ultrahigh energy density [12]. The oxygen vacancies with relatively low formation energies can also play a critical role in determining the surface and electronic properties of $SrTiO_3$. Experimental and theoretical studies have proved that the lowest energy charge state for oxygen vacancies with chemical stability is +2 in the vast majority of conditions [5, 14, 15]. Based on the assumption that oxygen vacancies in $SrTiO_3$ carry positive charges, Chiang *et al* proposed that oxygen vacancies provide the dominant contribution to tilting grain boundaries by the positive core charge in $SrTiO_3$ [13].

Oxygen vacancies are inescapably introduced into polycrystalline ceramics during sintering at high temperature in particular [8, 9] and therefore generally speaking, the density of oxygen vacancies is significantly lower in single crystals. It is recently reported that plasma-treated $SrTiO_3$ crystals exhibit different photocatalytic properties in relation to crystalline anisotropy [3]. The correlation barrier hopping has been found to be prevailing in the conduction mechanism of crystals [10]. The analysis of Fe:STO/Nb:STO heterostructure shows that electron hopping through localized defect states such as oxygen vacancies within the band gap is dominant at reverse and low forward bias [14]. Using anelastic relaxation measurements, two main relaxation mechanisms in oxygen deficient $SrTiO_3$ are identified with hopping of isolated oxygen vacancies over a barrier of 0.60 eV and reorientation of pairs of vacancies involving a barrier of 0.97 eV [15]. Although the properties of bulk $SrTiO_3$ have been quite well understood, the formation and migration of oxygen vacancies in $SrTiO_3$ single crystals with different crystal orientations are less clear. Herein, thermally stimulated depolarization current (TSDC) was selected to assist in the analysis of relaxation and degradation processes further. TSDC has been proved an enormous capacity for evaluating the qualitative and quantitative information of defects [16]. This effective experimental technique can complement other electrical characterization methods such as impedance spectroscopy to monitor defect behavior and loss mechanism of the materials [17]. Liu *et al* identified three peaks appearing in the TSDC spectra curves associated with the defect dipoles, trapped charges, and oxygen vacancies motion of the Fe-$SrTiO_3$ single crystals respectively. All these defect relaxation phenomena link to the degradation process [2, 17]. Understanding the behavior of oxygen vacancies is of particular importance to the study of degradation and reliability of capacitive dielectrics.

In recent years, well-defined single crystal surfaces of perovskite oxides typified by $SrTiO_3$ have been extensively investigated. Kawasaki *et al* obtained TiO_2 atomic plane terminated $SrTiO_3$ (100) for the first time by treating the crystal surface with a pH-controlled NH_4F-HF solution, and the terminating atomic layer could be tuned to the SrO atomic plane by homoepitaxial growth [18], while Koster *et al* further elevated the approach to get perfect and single terminated surfaces [19]. Hwang *et al* found two-dimensional electron gas with high mobility at $LaAlO_3$ and $SrTiO_3$ interface as the result of polarity discontinuities at the interfaces between different crystalline materials, namely heterointerfaces [20]. Since then, with the explosive development of experimental preparation methods, theoretical studies represented by first-principles in various types of interface and surface reconstruction of $SrTiO_3$ have also been put forward. Strong electron-electron and electron-lattice interactions near interface produce many new electronic effects, including metallic and ferromagnetic, superconductivity and quantum anomalous Hall effect [21–23]. In this work, first-principles DFT calculations were carried out on understanding the behavior of oxygen vacancies in $SrTiO_3$ (110) with different surface terminations. Based on the TSDC and first-principles calculation results, the behaviors of oxygen vacancies in $SrTiO_3$ single crystals under different conditions are elucidated, and the important role of oxygen vacancies in dielectric properties of $SrTiO_3$ is clarified.

2. Methods

2.1. Materials and experimental procedure

$SrTiO_3$ single crystals [$5 \times 5 \times 0.5$ mm; with face parallel to (100), (110), (111)] were grown by the Verneuil method, and the starting materials were purchased from the Shinkosha Co., Ltd (Yokohama, Japan) (figure 1). The Verneuil method, also called flame fusion method, is a technique of manufacturing synthetic crystals [24]. The chief process of the method involves melting a finely powdered highly pure starting material using an oxyhydrogen flame of at least 2000 °C at its core, and crystallizing the melted droplets into a boule. Once removed from the furnace and allowed to cool, the boule was split along its vertical axis to relieve internal pressure so as not to fracture. Both sides of all the samples were polished and then cleaned with plasma cleaner. For electrical measurements, Au electrodes were sputtered onto the top and bottom faces of $SrTiO_3$ single crystals. In TSDC characterizations, firstly samples were polarized at a fixed temperature T_p (100 °C $\leqslant T_p \leqslant$ 325 °C) and electric field E_p (50 V mm^{-1} $\leqslant E_p \leqslant$ 400 V mm^{-1}) for a period of time (10 min). Then, samples were rapidly cooled down to a starting temperature (−100 °C), while maintaining the electric field and depolarized for 10 min Finally, the electrodes were short-circuited and the released depolarization currents were recorded by a pA meter (6517B; Keithley, Cleveland, OH, USA) while heating the samples at a constant rate of 6 °C/min. The TSDC was recorded as a function of temperature with the aid of a quatro temperature controller of Novocontrol Technologies (Montabaur, Germany). The same batch of $SrTiO_3$ crystals with different orientations of (100), (110) and (111) were chosen to expose in O_2 atmosphere. $SrTiO_3$ single crystals were placed into the O_2 gas in the flow rate and heated at 800 °C for 30 h.

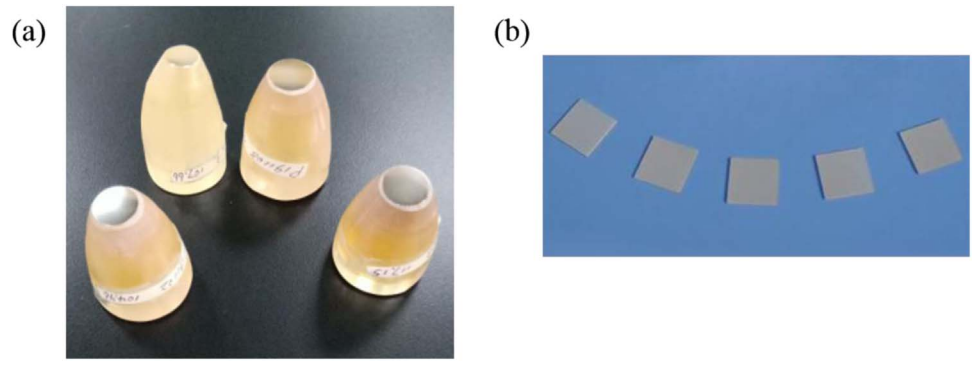

Figure 1. Photograph of (a) starting materials and (b) grown crystals cut into slabs of $SrTiO_3$.

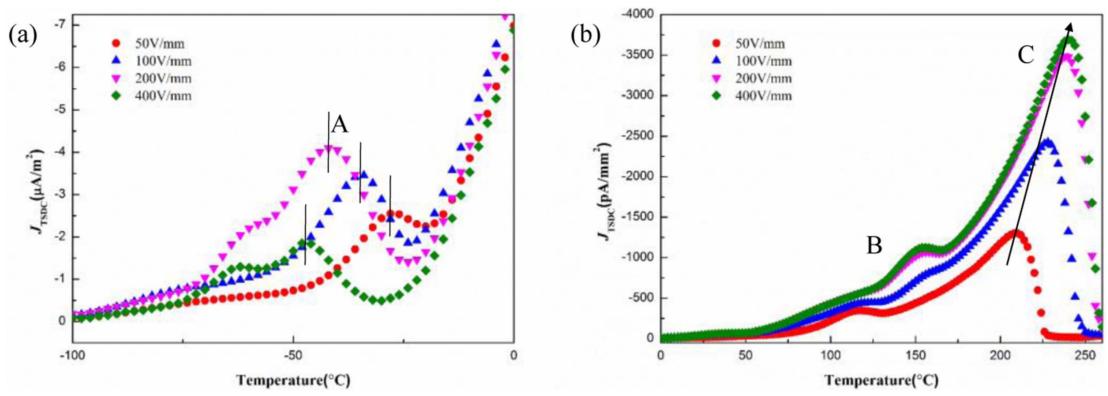

Figure 2. (a) Low-temperature and (b) high-temperature part of thermally stimulated depolarization current (TSDC) spectra for $SrTiO_3$ (110) crystal under a fixed polarization temperature (T_p) of 150 °C and varied polarization field (E_p) of 50–400 V mm^{-1}.

2.2. Computational details

$SrTiO_3$ (110) surfaces with oxygen defects were built based on cubic $SrTiO_3$ 2 × 2 × 3 supercells, which has a lattice parameter of 3.905 Å. A vacuum layer with the thickness of 12 Å was added to all the slabs. All calculations of surfaces and defects were performed from density functional theory (DFT) based on first-principles calculations as implemented Vienna *ab initio* simulation program (VASP) [25–27]. Generalized gradient approximation (GGA) with the PBE exchange-correlation functional for solid was adopted. To obtain accurate lattice parameters and band gaps, the semi local meta GGA functional was used to relax the lattice [28, 29]. The atomic positions were relaxed until the energy tolerance was 1 × 10^{-8} eV/atom and the maximum component of the force on any atom was smaller than 0.001 eV/Å. SCAN meta GGA functional and HSE06 functional were used to calculate the band structure. The HSE functional is composed of 25% Hartree–Fock (HF) exchange and 75% of GGA-PBE [30–32]. A Monkhorst-Pack mesh grid of 2 × 3 × 1 was employed, while the cut-off energy was chosen to be 600 eV [33]. The pseudopotentials used for surface slabs were constructed by the electron configurations as Sr $4s^2 4p^6 5s^2$ states, Ti $3s^2 sp^6 3d^2 4s^2$ states, and O $2s^2 2p^4$ states.

3. Results and discussion

Figure 2 displays the TSDC spectra curves for $SrTiO_3$ (110) single crystal polarized at different T_p of −100 °C–250 °C under a fixed DC E_p of 100 V mm^{-1}. A^{-1} s^{-1} the TSDC peak value J_m of high temperature part is several orders of magnitude higher than that of low temperature part, the spectra curve are divided into two segments, namely, −100 °C–0 °C and 150 °C–250 °C so as to better reflect the dependence of TSDC curves on polarization temperature. Each TSDC curve contains three distinct peaks (labeled A, B, and C), showing that at least three kinds of defect relaxation mechanisms exist in $SrTiO_3$ (110). For peak A at low temperature, position T_m of temperature corresponding to the TSDC peak decreases with increasing T_p, suggesting that peak A is most likely related to the relaxation of trap charge. This indicates that the TSDC relaxation of $SrTiO_3$ might have different physical mechanisms from TiO_2 or other Ti-containing ceramics in the same low temperature range [8]. Liu *et al* estimated that the trap charge concentration falls in the order of 10^{14} cm^{-3} in Fe-Doped $SrTiO_3$

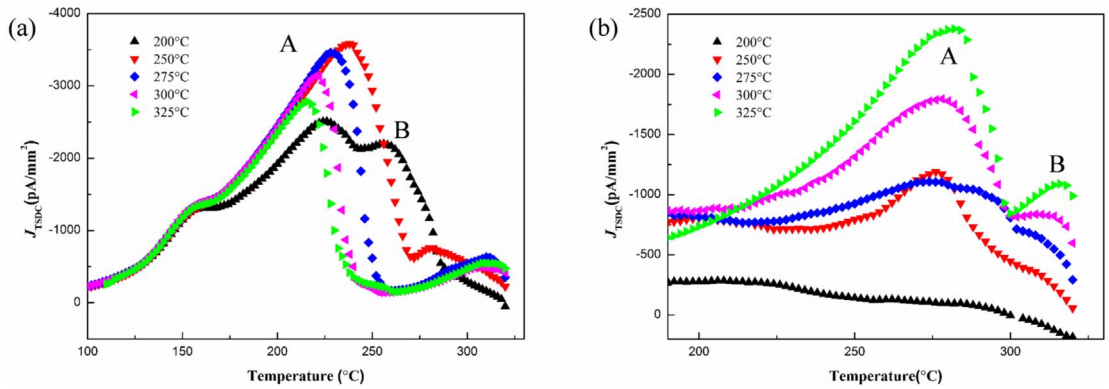

Figure 3. High-temperature part of thermally stimulated depolarization current (TSDC) spectra for $SrTiO_3$ (110) crystal (a) without and (b) with oxygen atmosphere treatment under a fixed polarization field (E_p) of 100 V mm^{-1} and varied polarization temperature (T_p) of 200 °C–325 °C.

single crystals, which is far less than that of defect dipoles [2]. With increasing T_p, T_m does not change much for peak B, indicating that peak B is probably originated from the relaxation of defect dipoles. Both T_m and J_m initially increase and then become saturated for peak C. This result illustrates that peak C is most likely generated from the relaxation of oxygen vacancies, just as that of occurring in polycrystalline located in grains. In single crystal samples, when the polarization conditions including T_p and E_p are improved to the saturation degree, the level of oxygen vacancies migration in the crystal grains will reduce and the TSDC peak values will decrease. As single crystals can eliminate the factors in the movement of oxygen vacancies through grain boundaries [8, 34], the effect of crystal orientations on the behaviors of oxygen vacancies can be well studied. The results of our research indicate that the J_m of peak A is far below peak B and C appearing at higher temperature part. It means that oxygen vacancies and secondly defect dipoles are the dominant origins of relaxation in $SrTiO_3$ single crystals.

With increasing T_p, as illustrated in figure 3(a), T_m and J_m initially increase and then become saturated and decrease for peak A. T_m of peak B shifts to higher values while J_m shows a decrease as T_p increases. To gain better insight into the possible origins of these relaxations, the dependence between polarization temperature T_p and T_m as well as J_m of peak A is shown in figure 4. By contrast, both temperature peak A and B position in figure 3(b) are less dependent on T_p (figure 4(a)) after the treatment of oxygen atmosphere. Meanwhile, the TSDC peak absolute values J_m of both peaks increase consistently. This is due to the decrease of oxygen vacancy concentration in crystals by heating the sample in oxygen. These results demonstrate that oxygen vacancies are also introduced into single crystals by the flame fusion method. The saturation of J_m with oxygen atmosphere treatment also disappears. According to the initial rise method [35], the activation energy E_a can be determined by using the following simplified equation:

$$\ln|J(T)| \cong C - \frac{E_a}{kT} \tag{1}$$

where T is the absolute temperature, $J(T)$ is the depolarization current density as a function of T, and C is a constant independent of temperature. By plotting ln$J$ against $1/T$ in the temperature rise of the initial current of TSDC peaks, the depth of defects such as the activation energy E_a of oxygen vacancies in dielectric materials can be estimated. The fitting results of $SrTiO_3$ (110) crystals under a fixed E_p of 100 V mm^{-1} and varied T_p for peak A in figure 3 are depicted in figure 5. The calculated E_a values are 0.55–0.57 eV (all with uncertainties of 0.01 eV) without O_2 treatment and 0.25–0.45 eV (with uncertainties of 0.01–0.03 eV) with O_2 treatment, respectively. Based on the above points, the activation of oxygen vacancies is easier after oxygen atmosphere treatment. Besides, the relaxation behaviors in the oxygen-treated samples tilt towards the orientation of defect dipoles. The motion of an oxygen vacancy perhaps plays the role as the movement of a local associated dipole in the aging and fatigue processes of ferroelectrics [2]. The most probable dipole in our systems is (Ti_{Ti}')–$(V_O^{\cdot\cdot})$ caused by the interactions between oxygen vacancies and hopping of valence-variable charged Ti [8, 36, 37].

For the same type of the peak in the TSDC curves of $SrTiO_3$ with three crystal orientations, J_m of $SrTiO_3$ (110) are higher than that of $SrTiO_3$ (100) and $SrTiO_3$ (111) peak under identical polarization and atmosphere treatment conditions. For instance, when $T_p = 150$ °C and $E_p = 300$ V mm^{-1}, J_m of $SrTiO_3$ (110) is approximately 1280 pA mm^{-2}, while it is 823 pA mm^{-2} for $SrTiO_3$ (111) (figures 6(a), (b)). On the other hand, contrasting figure 3(b) with figure 6(c), when $T_p = 150$ °C and $E_p = 300$ V mm^{-1}, J_m of $SrTiO_3$ (110) is about 1800 pA mm^{-2}, while it is 651 pA mm^{-2} for $SrTiO_3$ (100). On the basis of the Langevin function [35], the concentration of oxygen vacancies in $SrTiO_3$ (110) is higher than in $SrTiO_3$ (100) and $SrTiO_3$ (111). In addition,

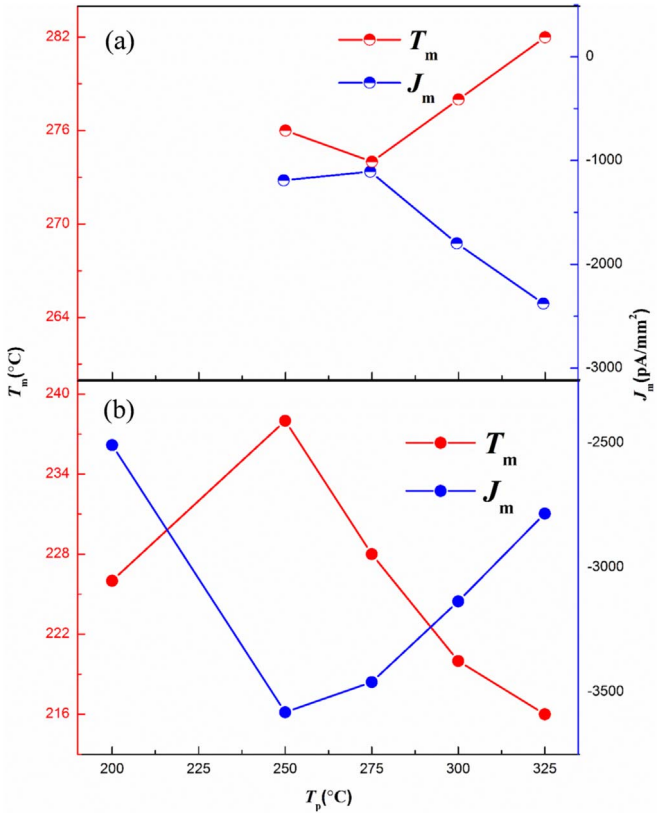

Figure 4. The dependence of thermally stimulated depolarization current (TSDC) relaxation peak A positions (T_m and J_m) under different polarization temperature for $SrTiO_3$ (110) crystals (a) with and (b) without oxygen atmosphere treatment.

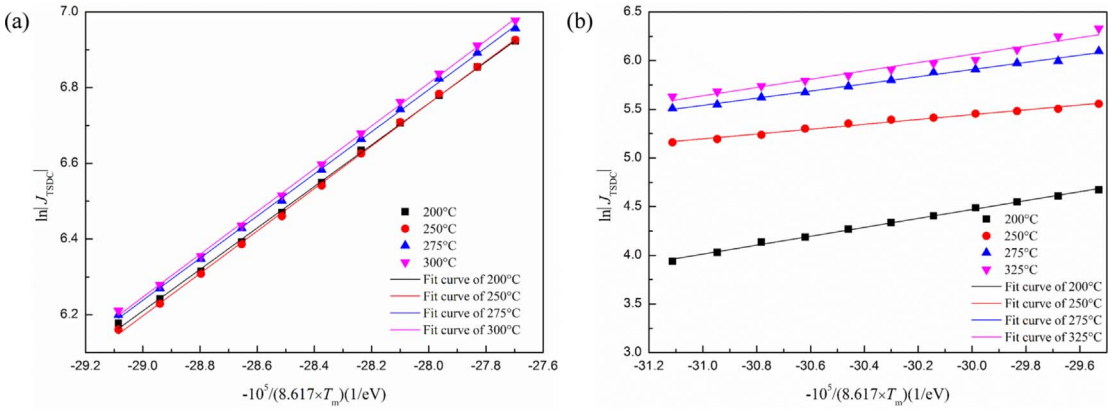

Figure 5. The fitting results of thermally stimulated depolarization current (TSDC) relaxation peak A for $SrTiO_3$ (110) crystals (a) without and (b) with O_2 treatment under a fixed polarization field (E_p) of 100 V mm^{-1} and varied polarization temperature (T_p) of 200 °C–325 °C using the initial rise method.

the calculated activation energy E_a of $SrTiO_3$ (110) is larger than the other two crystal orientations as well. Comparing the above results of the E_a 0.55 ± 0.01–0.57 ± 0.01 eV for $SrTiO_3$ (110), the calculated E_a values are 0.39 ± 0.02–0.44 ± 0.01 eV for $SrTiO_3$ (111) and 0.25 ± 0.02–0.31 ± 0.01 eV for $SrTiO_3$ (100) without O_2 treatment, respectively. In contrast with literatures [2, 17, 38], the calculated activation energies are small to some extent, mainly because of the influence of other defect relaxations and different doping conditions. This raises an important point that defect relaxation associated with oxygen vacancies should exist crystalline anisotropy. It is assumed that the anisotropy is mainly related to the surface effect, especially the migration of oxygen vacancies through the electrode–crystal interface. The TiO_6 octahedra can significantly influence the

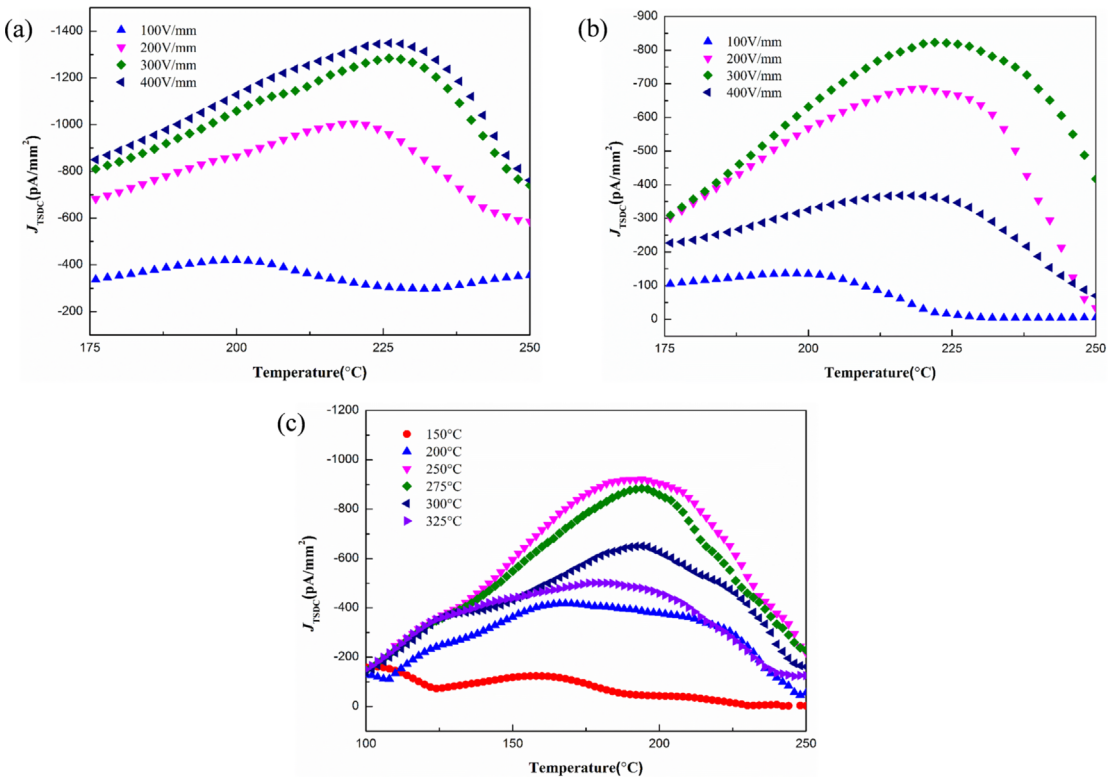

Figure 6. High-temperature part of thermally stimulated depolarization current (TSDC) spectra for $SrTiO_3$ single crystals with oxygen atmosphere treatment: (a) $SrTiO_3$ (110), (b) $SrTiO_3$ (111) under a fixed polarization temperature (T_p) of 150 °C and varied polarization field (E_p) of 100–400 V mm^{-1} and (c) $SrTiO_3$ (100) under a fixed E_p of 100 V mm^{-1} and varied T_p of 150 °C–325 °C.

defect behaviors in Ti-containing materials [8]. For the $SrTiO_3$ crystals with different orientations, the interaction between oxygen vacancies and different arranged TiO_6 octahedra near the surface is not entirely identical, thus resulting in distinct relaxation performance.

From the TSDC characterization, we have analyzed the feature of TSDC spectra in order to recognize various types of defect relaxation in $SrTiO_3$ single crystals and found the difference between three distinct crystal orientations therein. However, the distinction of $SrTiO_3$ surface microstructure with different terminated atoms cannot be separated from the experiment. Furthermore, the mechanisms of defects formation and relaxation along with their influence upon transportation of carriers in perovskite oxides are ambiguous. Owing to the comparatively vivid and complete TSDC spectra of $SrTiO_3$ (110), first-principles density functional theory calculations were used to investigate structural and dielectric behaviors of oxygen vacancies in $SrTiO_3$ (110) crystals in order to make a profound research on these problems. Firstly, the structural and electronic properties for bulk $SrTiO_3$ lattice were calculated. The relaxed lattice parameter is 3.898 Å, which is in good agreement (~0.18% error) with the experimental (3.905 Å) [39, 40] and other theoretical results [41, 42]. The calculated band gap for bulk $SrTiO_3$ lattice was 1.81 eV from the GGA-PBE functional. It is well known that calculations derived from GGA functional underestimate the band gaps. Using the latest meta GGA functional SCAN, the band gap is 2.8 eV. Using the HSE06 functional, the band gap is 3.2 eV, same with the experimental value of 3.2 eV [43]. The relaxed lattice parameter was adopted for the surface calculations and defect calculations.

The $SrTiO_3$ (110) surface slabs were built on the cleavage of $SrTiO_3$ 2 × 2 × 3 supercell. Three types of surface slabs were modelled and one oxygen atom was removed from the top layer of each slab. The resulted threes slabs are O-terminated, TiO-terminated, and Sr-terminated lattice as shown in figure 7. The calculated formation energy of oxygen vacancies is 1.43 eV and 2.17 eV for O-terminated surfaces and Sr-terminated surfaces, respectively. For the case of TiO-terminated surfaces, the formation energy of oxygen vacancies is 0.63 eV, which is consistent with the calculated E_a values in the above-mentioned TSDC fitting results. In fact, apart from formation energy, activation energy E_a evaluated from the relaxation process should include migration energy or hopping barrier of oxygen vacancies. As mentioned earlier, the activation energies calculated from the fitting results of TSDC are relatively low. In addition, because the oxygen vacancies in our atomic structure model are close to the surface, the formation energies may be considerably underestimated

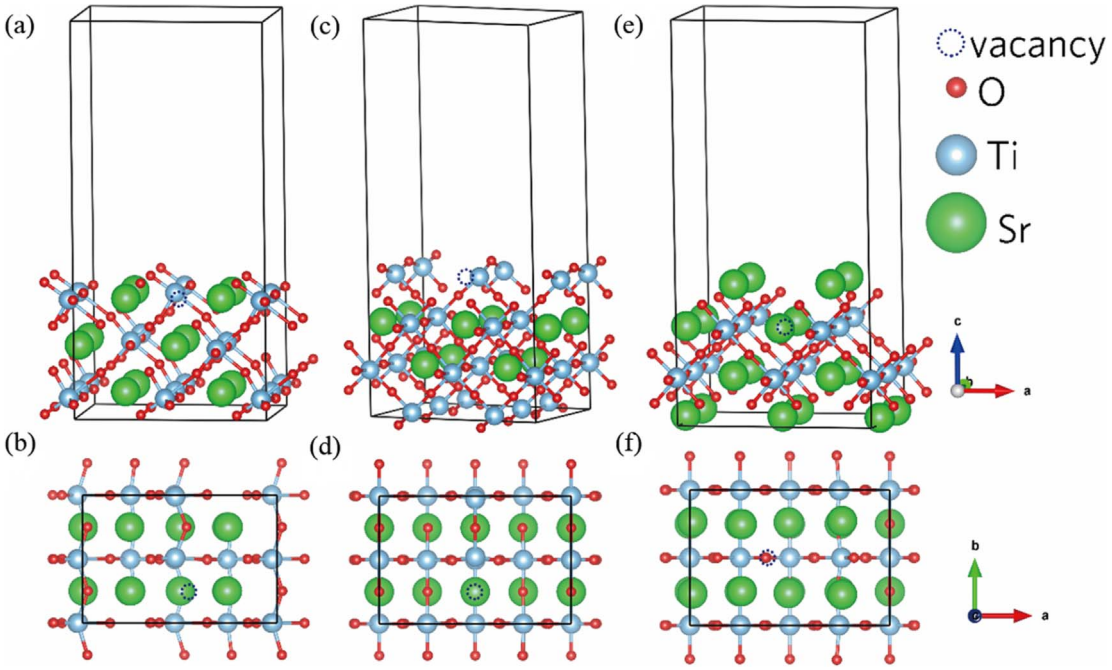

Figure 7. Relaxed lattice structure of $SrTiO_3$ (110) surfaces with oxygen vacancy. (a), (b) O-terminated, (c), (d) TiO-terminated, (e), (f) Sr-terminated surfaces. The dotted circles represent the oxygen vacancies.

compared with the overall sample. In brief, thus it can be concluded that the oxygen vacancies form relatively easily on the TiO-terminated surfaces.

Figures 8 and 9 show the band structure and density of states of $SrTiO_3$ (110) surfaces with different terminations and oxygen vacancies. For the case of $SrTiO_3$ (110) surfaces with different terminations containing no oxygen vacancies, all the band structures show insulator band gaps. For instance, the O-terminated and TiO-terminated surface slabs display band gaps around 2 eV, while the Sr-terminated surface slabs display a band gap of 1.6 eV. The introduction of oxygen vacancies on O-terminated surface slabs enlarges the band gap to 3.6 eV. In the case of Sr-terminated surface slabs, the oxygen vacancies enlarge the band gap to 1.8 eV. As shown in figures 8(b), (d), (f)), the Fermi level is crossing the conduction band minimum. For the case of O-terminated and TiO-terminated surfaces, some medium bands appear between conduction band and valence band due to the introduction of oxygen vacancies. The introduction of oxygen vacancies on the corresponding surfaces induces the transition from insulator to metallic behavior. It indicates that one of the important sources of the space charge current through $SrTiO_3$ single crystals is considered to be from the relaxation of oxygen vacancies occurring near the surface, which is the most mobile ions in the $SrTiO_3$ system [2]. These analysis conclusions are well complementary for our experimental study in preceding sections. The introduction of oxygen vacancies in first-principles calculation models can correspond to $SrTiO_3$ samples without oxygen treatment, while the absence of oxygen vacancy could be approximately considered as $SrTiO_3$ samples with thorough oxygen treatment. After applied oxygen, $SrTiO_3$ crystals possess lower concentration of oxygen vacancies and better insulation.

4. Conclusions

In summary, we have studied the thermal relaxation behaviors of oxygen vacancies and other related defects in the $SrTiO_3$ single crystals by TSDC spectra. Different sources of relaxation stemming from oxygen vacancy motion, trap charges and defect dipoles are identified and evaluated. It has been shown that the oxygen-treated $SrTiO_3$ crystals have lower concentration and activation energy of oxygen vacancies. Furthermore, oxygen vacancies probably prefer to combine with other defect ions to form the defect association. Experimental evidence of the anisotropy of relaxation behaviors in relation to oxygen vacancies has been given. The $SrTiO_3$ (110) samples display higher concentration and activation energy of oxygen vacancies than other orientations. By using first-principles DFT calculations, we studied the stability of $SrTiO_3$ (110) with different atoms terminated surface. Comparisons between different surface microstructure suggest that the oxygen vacancies form relatively easily on the TiO-terminated surfaces. The trend of transition from insulator to metallic behavior

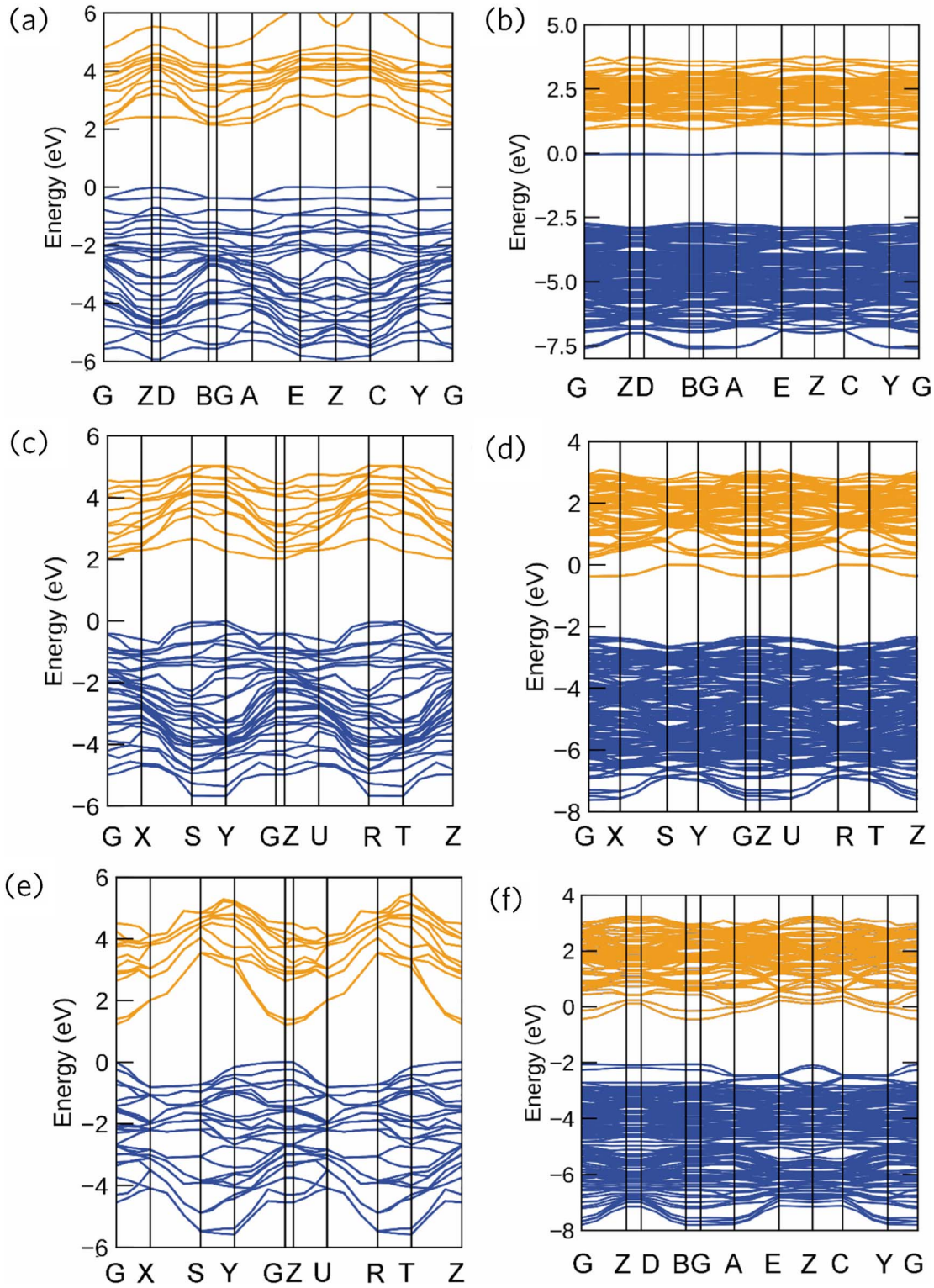

Figure 8. Band structure of $SrTiO_3$ (110) surfaces with different terminations and oxygen vacancies. O-terminated surfaces (a) without and (b) with oxygen vacancies, TiO-terminated surfaces (c) without and (d) with oxygen vacancies, Sr-terminated surfaces (e) without and (f) with oxygen vacancies.

of $SrTiO_3$ surface is originated from oxygen vacancies, and it provides a potential origin of leakage current. This phenomenon may have an underlying theoretical prospect for applications in novel components. These findings are expected to inspire us and other researchers to make further investigation on applying various techniques such as TSDC and first-principles calculations to perovskite oxides or other dielectrics. Our efforts would help to gain a better understanding in degradation and aging of $SrTiO_3$ or other capacitive materials under different levels and stages.

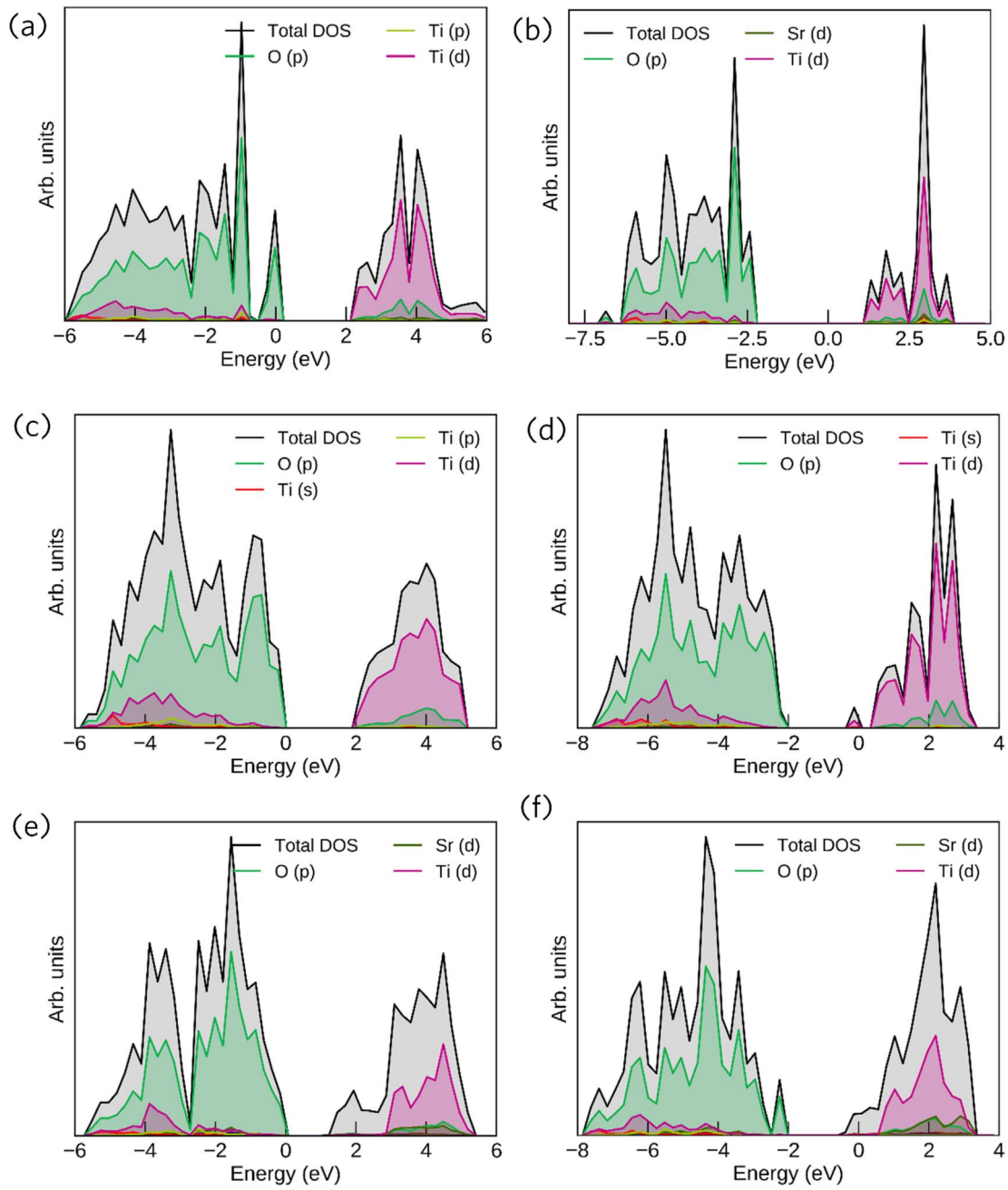

Figure 9. Density of states of various $SrTiO_3$ (110) surfaces (a), (c), (e) without and (b), (d), (f) with oxygen vacancies. (a) O-terminated surface without defects; (b) O-terminated surface with defects; (c) TiO-terminated surface without defects; (d) TiO-terminated surface with defects; (e) Sr-terminated surface without defects; (f) Sr-terminated surface with defects. Fermi level is set to be zero.

Acknowledgments

This work was supported by the National Key Research and Development Program of China (Grant No.2017YFB0406301), and the National Natural Science Foundation of China (Grant No. 51872160).

ORCID iDs

Haimo Qu https://orcid.org/0000-0002-6762-1130

References

[1] Buchanan R 2004 *Ceramic Materials for Electronics, 3rd Edition* (Boca Raton: CRC Press) (https://doi.org/10.1201/9781315273242)
[2] Liu W and Randall C 2008 Thermally Stimulated Relaxation in Fe-Doped $SrTiO_3$ Systems: II. Degradation of $SrTiO_3$ Dielectrics *J. Am. Ceram. Soc.* **91** 3251–7

[3] Zhao H, Fan Z, Fu Q, Wang H, Hu Z, Tao H, Zhang X, Ma Z and Jia T 2018 Enhanced photocatalytic performance of $SrTiO_3$ crystals with (100), (110) and (111) orientations treated by N_2 (H_2) plasma *J. Mater. Sci.* **53** 15340–7
[4] Konta R, Ishii T, Kato H and Kudo A 2004 Photocatalytic activities of noble metal ion doped $SrTiO_3$ under visible light irradiation *J. Phys. Chem. B* **108** 8992–5
[5] Behtash M, Wang Y, Luo J and Yang K 2018 Oxygen vacancy formation in the $SrTiO_3$ R5 [001] twist grain boundary from first-principles *J. Am. Ceram. Soc.* **101** 3118–29
[6] Luo Y, Liu X, Li X and Chen G 2007 $BaBiO_3$-doped $SrTiO_3$-based NTC thermistors *J. Alloy. Compd.* **433** 221–4
[7] Maier R, Pomorski T, Lenahan P and Randall C 2015 Acceptor-oxygen vacancy defect dipoles and fully coordinated defect centers in a ferroelectric perovskite lattice: electron paramagnetic resonance analysis of Mn^{2+} in single crystal $BaTiO_3$ *J. Appl. Phys.* **118** 164102
[8] Zhang J, Yue Z, Luo Y, Zhang X and Li L 2017 Understanding the thermally stimulated relaxation and defect behavior of Ti-containing microwave dielectrics: A case study of $BaTi_4O_9$ *Materials & Design* **130** 479–87
[9] Pullar R, Penn S, Wang X, Reaney I and Alford N 2009 Dielectric loss caused by oxygen vacancies in titania ceramics *J. Eur. Ceram. Soc.* **29** 419–24
[10] Joshi J, Joshi G, Joshi M, Jethva H and Parikh K 2018 Raman, photoluminescence, and a.c. electrical studies of pure and l-serine doped ammonium dihydrogen phosphate single crystals: an understanding of defect chemistry in hydrogen bonding *New J. Chem.* **42** 17227–49
[11] Joshi J, Kanchan D, Jethva H, Joshi M and Parikh K 2018 Dielectric relaxation, protonic defect, conductivity mechanisms, complex impedance and modulus spectroscopic studies of pure and L-threonine-doped ammonium dihydrogen phosphate *Ionics* **24** 1995–2016
[12] Hou C, Huang W, Zhao W, Zhang D, Yin Y and Li X 2017 Ultrahigh energy density in $SrTiO_3$ film capacitors *ACS Appl. Mater. Interfaces* **9** 20484–90
[13] Chiang Y and Takagi T 1990 Grain-boundary chemistry of barium titanate and strontium titanate: I, high-temperature equilibrium space charge *J. Am. Ceram. Soc.* **73** 3278–85
[14] Saraf S, Riess I and Rothschild A 2016 Parallel band and hopping electron transport in $SrTiO_3$ *Adv. Electron. Mater.* **2** 1500368
[15] Cordero F 2007 Hopping and clustering of oxygen vacancies in $SrTiO_3$ by anelastic relaxation *Phys. Rev. B* **76** 172106
[16] Zhang J, Yue Z and Li L 2017 Crystal structure, defect relaxation, and microwave dielectric properties of $Ba[(Mg_{1/3}Nb_{2/3})_{1-x}Hf_x]O_3$ solid solutions *J. Am. Ceram. Soc.* **101** 1974–81
[17] Liu W and Randall C 2008 Thermally stimulated relaxation in Fe-Doped $SrTiO_3$ systems: I. single crystals *J. Am. Ceram. Soc.* **91** 3245–50
[18] Kawasaki M, Takahashi K, Maeda T and Tsuchiya R 1994 Atomic control of the $SrTiO_3$ crystal surface *Science* **266** 1540–2
[19] Koster G, Kropman B, Rijnders G, Blank D and Rogalla H 1998 Quasi-ideal strontium titanate crystal surfaces through formation of strontium hydroxide *Appl. Phys. Lett.* **73** 2920–2
[20] Ohtomo A and Hwang H 2004 A high-mobility electron gas at the $LaAlO_3/SrTiO_3$ heterointerface *Nature* **27** 423–6
[21] Okamoto S and Millis A 2004 Electronic reconstruction at an interface between a Mott insulator and a band insulator *Nature* **428** 630–3
[22] Biscaras J, Bergeal N, Kushwaha A, Wolf T, Rastogi A and Budhani R 2010 Two-dimensional superconductivity at a Mott insulator/band insulator interface $LaTiO_3/SrTiO_3$ *Nat. Commun.* **1** 1–5
[23] Wang Y, Wang Z, Fang Z and Dai X 2015 Interaction-induced quantum anomalous Hall phase in (111) bilayer of $LaCoO_3$ *Phys. Rev. B* **91** 125139
[24] Scheel H 2000 Historical aspects of crystal growth technology *J. Cryst. Growth* **211** 1–12
[25] Kresse G and Joubert D 1999 From ultrasoft pseudopotentials to the projector augmented-wave method *Phys. Rev. B* **59** 1758–75
[26] Blöchl P 1994 Projector augmented-wave method *Phys. Rev. B* **50** 17953–79
[27] Kresse G and Furthmüller J 1996 Efficient iterative schemes for ab initiototal-energy calculations using a plane-wave basis set *Phys. Rev. B* **54** 11169–86
[28] Sun J, Xiao B, Fang Y, Haunschild R, Hao P, Ruzsinszky A, Csonka G, Scuseria G and Perdew J 2013 Density functionals that recognize covalent, metallic, and weak bonds *Phys. Rev. Lett.* **111** 106401
[29] Charles N and Rondinelli J 2016 Assessing exchange-correlation functional performance for structure and property predictions of oxyfluoride compounds from first principles *Phys. Rev. B* **94** 174108
[30] Heyd J, Scuseria G and Ernzerhof M 2003 Hybrid functionals based on a screened Coulomb potential *J. Chem. Phys.* **118** 8207–15
[31] Krukau A, Vydrov O, Izmaylov A and Scuseria G 2006 Influence of the exchange screening parameter on the performance of screened hybrid functionals *J. Chem. Phys.* **125** 1–5
[32] Perdew J, Ruzsinszky A, Csonka G, Vydrov O, Scuseria G, Constantin L, Zhou X and Burke K 2007 Generalized gradient approximation for solids and their surfaces *Phys. Rev. Lett.* **100** 136406
[33] Monkhorst H and Pack J 1976 Special points for Brillouin-zone integrations *Phys. Rev. B* **13** 5188–92
[34] Liu W 2009 *Impedance/thermally Stimulated Depolarization Current and Microstructural Relations at Interfaces in Degraded Perovskite Dielectrics* The Pennsylvania State University (PhD Dissertation) (https://search.proquest.com/docview/304983009?accountid=14426)
[35] Braunlich P 1979 *Thermally Stimulated Relaxation in Solids* (Berlin, Heidelberg: Springer) (https://doi.org/10.1007/3-540-09595-0)
[36] Zhang J, Yue Z, Zhou Y, Peng B, Zhang X and Li L 2016 Temperature-dependent dielectric properties, thermally-stimulated relaxations and defect-property correlations of TiO_2 ceramics for wireless passive temperature sensing *J. Eur. Ceram. Soc.* **36** 1923–30
[37] Zhang J, Yue Z, Zhou Y, Zhang X and Li L 2015 Microwave dielectric properties and thermally stimulated depolarization currents of $(1–x)MgTiO_3–xCa_{0.8}Sr_{0.2}TiO_3$ ceramics *J. Am. Ceram. Soc.* **98** 1548–54
[38] Fukami T, Kusunoki M and Tsuchiya H 1987 TSC study on iron doped barium–strontium titanate ceramics *Jap. J. Appl. Phys.* **26** 46–9
[39] Longo V, das Graça Sampaio Costa M, Zirpole Simões A, Rosa I, Santos C, Andrés J, Longo E and Varela J 2010 On the photoluminescence behavior of samarium-doped strontium titanate nanostructures under UV light. A structural and electronic understanding *Phys. Chem. Chem. Phys.* **12** 7566–79
[40] Mitchell R, Chakhmouradian A and Woodward P 2000 Crystal chemistry of perovskite-type compounds in the tausonite-loparite series, $(Sr_{1-2x}Na_xLa_x)TiO_3$ *Phys. Chem. Miner.* **27** 583–9
[41] Eglitis R and Vanderbilt D 2008 First-principles calculations of atomic and electronic structure of $SrTiO_3$ (001) and (011) surfaces *Phys. Rev. B* **77** 195408
[42] Bottin F, Finocchi F and Noguera C 2003 Stability and electronic structure of the (1×1) $SrTiO_3$ (110) polar surfaces by first-principles calculations *Phys. Rev. B* **68** 035418
[43] Benthem K, Elsässer C and French R 2001 Bulk electronic structure of $SrTiO_3$: Experiment and theory *J. Appl. Phys.* **90** 6156–64

[44] Astala R and Bristowe P 2001 *Ab initio* study of the oxygen vacancy in $SrTiO_3$ *Model. Simul. Mater. Sci.* **9** 416–22
[45] Buban J, Iddir H and Öğüt. S 2004 Structural and electronic properties of oxygen vacancies in cubic and antiferrodistortive phases of $SrTiO_3$ *Phys. Rev. B* **69** 180102